The FASEB Journal article fj.201600897RR. Published online November 8, 2016.

Mechanical remodeling of normally-sized mammalian cells under a gravity vector

Chen Zhang, Lüwen Zhou, Fan Zhang, Dongyuan Lü, Ning Li, Lu Zheng, Yanhong Xu, Zhan Li, Shujin Sun, and Mian Long[1]

Center for Biomechanics and Bioengineering, Key Laboratory of Microgravity (National Microgravity Laboratory), and Beijing Key Laboratory of Engineered Construction and Mechanobiology, Institute of Mechanics, Chinese Academy of Sciences, Beijing, China

ABSTRACT: Translocation of the dense nucleus along a gravity vector initiates mechanical remodeling of a cell, but the underlying mechanisms of cytoskeletal network and focal adhesion complex (FAC) reorganization in a mammalian cell remain unclear. We quantified the remodeling of an MC3T3-E1 cell placed in upward-, downward-, or edge-on–orientated substrate. Nucleus longitudinal translocation presents a high value in downward orientation at 24 h or in edge-on orientation at 72 h, which is consistent with orientation-dependent distribution of perinuclear actin stress fibers and vimentin cords. Redistribution of total FAC area and fractionized super mature adhesion number coordinates this dependence at short duration. This orientation-dependent remodeling is associated with nucleus flattering and lamin A/C phosphorylation. Actin depolymerization or Rho-associated protein kinase signaling inhibition abolishes the orientation dependence of nucleus translocation, whereas tubulin polymerization inhibition or vimentin disruption reserves the dependence. A biomechanical model is therefore proposed for integrating the mechanosensing of nucleus translocation with cytoskeletal remodeling and FAC reorganization induced by a gravity vector.—Zhang, C., Zhou, L., Zhang, F., Lü, D., Li, N., Zheng, L., Xu, Y., Li, Z., Sun, S., Long, M. Mechanical remodeling of normally-sized mammalian cells under gravity vector. FASEB J. 31, 000–000 (2017). www.fasebj.org

KEY WORDS: gravity-directed · mechanosensing · nucleus translocation · cytoskeletal remodeling · FAC reorganization

Cells on Earth are subject to a variety of mechanical forces, including gravity. Statolith, or amyloplast, has long been assumed to be a gravity receptor for plant species to sense, transduce, and respond to altered gravity (1); however, little is known about mechanisms that underlie gravisensing and gravitransduction in mammalian cells, even though a body of evidence confirms the effect of gravity on their biological responses (2). Conceptual studies have indicated that the spreading and mitosis of normally sized ($\sim 10^1$ μm) mammalian cells are sensitive to the change in gravity vector. For example, randomizing the direction of gravity has no effect on the division orientation of Chinese hamster ovary cells that are point-attached in a vertical plane (3). Inversion of culture substrate cannot alter the number and function of attached osteoblasts, even though an immediate response—diminished viable osteoblast number—is observed in sparse, early cultures (4). Cell area, nucleus translocation, cell cycle, and F-actin reorganization vary significantly in a duration-dependent manner when Ros 17/2.8 cells make up a monolayer and are spread on downward- or edge-on–orientated substrate compared with those on an upward orientation (5). More quantitative analysis is observed in large-sized *Xenopus* oocytes (~1 mm), where the nucleolus sedimentation is dominant compared with the thermal fluctuation at gravity potential > thermal energy scale (6), which implies that the sedimentation of a relatively dense nucleus could initiate gravisensing in a mammalian cell.

The simplest gravisensing model of a single cell is when the cytoskeleton senses gravitational force acting on or being lost from organelles. Generally, those dense organelles (*i.e.*, nuclei or mitochondria) do not sediment as a result of their attachment to cytoskeletal filaments and thus exert a force on the cytoskeleton. A body of evidence indicates that loss of gravity or of stimulated microgravity alters prestress in the cytoskeleton and is then transmitted to mechanosensitive structures. In this regard, actin is redistributed and has either a more perinuclear or more cortical localization. Microtubules lose their radial organization and tend to be shortened, more curved and bent,

ABBREVIATIONS: 3D, 3-dimensional; ALP, alkaline phosphatase; FAC, focal adhesion complex; FX, focal complex; RAPD, random amplified polymorphic DNA; ROCK, Rho-associated protein kinase; SMA, super mature adhesion

[1] Correspondence: Institute of Mechanics, Chinese Academy of Sciences, No. 15 North 4th Ring Rd., Beijing 100190, China. E-mail: mlong@imech.ac.cn

doi: 10.1096/fj.201600897RR

This article includes supplemental data. Please visit *http://www.fasebj.org* to obtain this information.

and localized perinuclearly. Intermediate filaments form clusters, larger meshes appear in the network, and their localization is likely perinuclear (2, 7–9). Thus, the cytoskeletal network is the preferential candidate to elucidate the mechanical stabilization of the dense organelle-induced sedimentation against gravity. This is not only because of the mechanical support of organelle sedimentation but also because of roles played in connecting the intracellular microenvironment to extracellular microenvironment. In an adherent mammalian cell, actin stress fibers are well formed under gravity in number, length, and thickness. To let the cell well adhere to substrate, focal adhesion complexes (FACs) align with stress fibers, distribute with radial orientation, and promote cell spreading *via* point attachment to the substrate (10–13). However, the major gravisensing axis of nucleus sedimentation–cytoskeletal remodeling–FAC rearrangement has not been explicitly elucidated for mammalian cells.

Although the force that is generated by polymerization of microtubules and actin or by a single molecular motor—on the order of several pN—is almost 10 times higher than that exerted by gravity for a normal-sized mammalian cell—on the order of 0.5 pN—it is still hard to definitively exclude the influence of gravity. This is because the integral effect of specific organelle sedimentation, which is attributed to the density difference between organelles and the cytoplasm, may not be negligible for long-term adherence to the surface, and/or the role of the cytoskeleton in gravisensing is fine-tuning during various steps of response. There are at least 3 exceptional cases of small, little-effect gravity: smaller forces applied over longer timescales could have effects that are similar to those of large forces on short timescales from mechanosensitive proteins (14, 15); cytoskeleton-exerted force could be concentrated on 1 or few mechanotransductive elements by the cytoskeleton (16); and active, nonthermal fluctuations could—*via* the mechanism of stochastic resonance—enhance the sensing of a small gravitational signal instead of masking it (17, 18).

Here, we hypothesized that the biological homeostasis of a mammalian cell on a gravity vector is maintained by the mechanical balance of nucleus sedimentation with cytoskeletal remodeling and FAC rearrangement on long timescales. By using an orientation-varied cell culture assay, previously described (3–5), we conducted detailed analyses for adherent MC3T3-E1 cells to unravel how a gravity vector governs mechanical stability, mainly from the viewpoints of nucleus sedimentation, cytoskeletal remodeling, and FAC rearrangement. Our results suggest that those gravisensing mechanisms in plant cells could be applicable to mammalian cells in a distinct way.

MATERIALS AND METHODS

Reagents and cells

FITC-conjugated phalloidin was purchased from Enzo Life Sciences (Farmingdale, NY, USA). Alexa Flour 555–conjugated anti–α-tubulin rabbit mAbs, Alexa Flour 647–conjugated anti-vimentin rabbit mAbs, anti–lamin A/C mouse mAbs, anti–p-lamin A/C rabbit mAbs, and Alexa Flour 647–conjugated goat anti-mouse anti-IgG secondary polyclonal Abs were from Cell Signaling Technology (Danvers, MA, USA). Anti-vinculin rabbit mAbs and Alexa Flour 488– or DyLight 594–conjugated donkey anti-rabbit and anti-IgG secondary polyclonal Abs were from Abcam (Cambridge, United Kingdom). Tetramethylrhodamine-labeled anti-paxillin mouse mAbs were from Becton Dickinson (Franklin Lakes, NJ, USA). Allophycocyanin-conjugated anti-CD29 (β1-integrin) hamster mAbs were from Biolegend (San Diego, CA, USA). Hoechst 33342 was obtained from Thermo Fisher Scientific (Waltham, MA, USA).

Mouse MC3T3-E1 preosteoblast cells, obtained from Peking Union Medical College Hospital (Beijing, China), were grown at 37°C in a 5% CO_2 incubator in α-minimal essential medium (GE Healthcare Life Sciences, Logan, UT, USA) that was supplemented with 10% fetal calf serum (Thermo Fisher Scientific), 2 mM L-glutamine (GE Healthcare Life Sciences), and 1% penicillin-streptomycin (GE Healthcare Life Sciences). Cells were cultured in flasks and routinely passaged before being transferred onto oriented coverslips.

Oriented cell culture assay

Cells were placed on 3 oriented coverslips and grown for 24 or 72 h, as previously described (5). In brief, glass coverslips (Corning, Corning, NY, USA) were cut into rectangle shapes with a culture area of 4.8 cm^2 and were precoated by collagen I in 4 $\mu g/cm^2$. Cells grown on the coverslip for a preset 24 h were then transferred to a customer-made coverslip holder in the respective upward, downward, or edge-on orientation (Supplemental Fig. S1*A*). Here, we simply named these orientations according to the angle between the outer normal vector of the substrate and the vector of gravity, which read 180, 0, or 90° for upward, downward, or edge-on orientation, respectively (**Fig. 1*A*, *B***). To minimize the effect of hydrostatic pressure that originated from 3 distinct orientations, the same volume of culture medium of 18 ml per dish was added to the 180 and 0° coverslips to maintain the same medium height. For cells grown on the 90° coverslip, 100 ml medium was added, which resulted in a maximum hydrostatic pressure difference of 12 mm H_2O between the cells at the bottom and the top of the coverslip. The impact of such pressure difference on cells was negligible (5).

Cell proliferation, cycle, and differentiation

To test the time course of cell proliferation, cells were seeded at a density of 5×10^2 cells/cm^2 for cell growth for up to 7 d. After being cultured in the oriented substrate for the given durations (24-, 48-, 72-, 96-, 120-, 144- and 168-h, respectively), cells were then digested by 0.25% trypsin and cell number was counted by Handheld Automated Cell Counter (Millipore, Billerica, MA, USA). Triplicate repeats were conducted in each orientation.

For cell-cycle measurement, cells were cultured in α-minimal essential medium without fetal bovine serum for a preset 24 h for cell synchronization in G_0/G_1 phase (approximately 85%). Cells were seeded at a density of 2×10^2 to $\sim 7.5 \times 10^3$ cells/cm^2 7-d growth to reach a similar 90% confluence at different time points. After trypsinizing cells, cell cycle was analyzed by flow cytometry (Becton Dickinson Franklin Lakes, NJ, USA) using CycleTest Plus DNA Reagent Kit (Becton Dickinson). Fluorescence histograms were obtained by using manufacturer-provided ModFit software (Verity Software House, Topsham, ME, USA). Tests were repeated in 2 independent runs with 5 coverslips for each run.

For cell differentiation tests, cells grown on coverslips were incubated with an osteogenic-induced medium of 10 nM dexamethasone (Sigma-Aldrich, St. Louis, MO, USA),

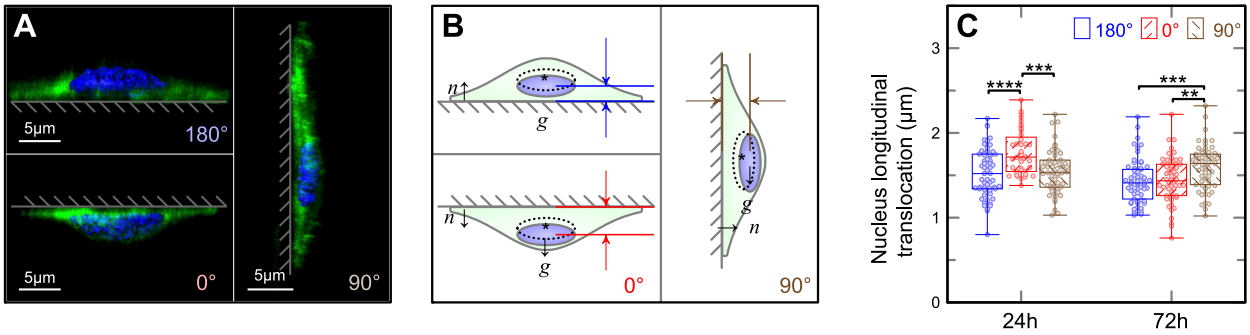

Figure 1. Gravity-directed translocation of MC3T3-E1 nucleus in 3 orientations. *A*) Typical image in respective orientation is illustrated by stained nucleus (blue) and actin (green). *B*) Nucleus longitudinal height is defined as the distance from nucleus centroid (*) to the substrate (nucleus contour is depicted as solid or dotted line at different time points; asterisk denotes cell centroid). *C*) Data are presented as median values with 25 and 75th percentiles of 40–60 cells from 3 experiments. $^{**}P < 0.01$; $^{***}P < 0.001$; $^{****}P < 0.0001$.

10 mM β-glycerophosphate, and 50 μg/ml ascorbic acid. Alkaline phosphatase (ALP) activity was determined by p-nitrophenylphosphate. Absorbance of the lysate was measured at 415 nm by using Bio-Rad reader (Hercules, CA, USA) and activity was calculated from a standard curve of total protein content of the lysate tested by Pierce BCA Protein Assay Kit (Thermo Fisher Scientific). Data were defined by the concentration (nM/min) and presented as ALP activity normalized by total protein content (nM/min/mg).

Cell morphology and cytoskeleton remodeling

Morphological changes and cytoskeletal expression were determined by using confocal microscopy. Here, cells were seeded at a density of 1×10^2 or 3×10^2 cells/cm^2 for 72 or 24 h to reach similar confluence with the majority of isolated cells. At 24 or 72 h, cells grown on oriented coverslips were washed with PBS, fixed for 15 min in 4% paraformaldehyde within 1 min, and permeated with 0.1% Triton X-100 for 10 min at room temperature. Collected cells were rinsed and incubated in 1% bovine serum albumin/PBS for 60 min at 37°C to block nonspecific staining. Filamentous actin, tubulin, and vimentin were stained with conjugated 5 μg/ml phalloidin, anti-tubulin mAbs at a dilution of 1:50, and anti-vimentin mAbs at a dilution of 1:800, respectively. After being incubated for 60 min at 37°C, cells were washed and incubated with Hoechst 33342 for 10 min to stain nuclei. Two- or 3-dimensional (3D) images of stained cells were examined using a confocal laser scanning microscope (LSM 710; Carl Zeiss AG, Oberkochen, Germany) with ×63 oil-immersion objective at a slicing height set of 0.65 μm in a stepwise interval of 0.322 μm for 3D imaging. Triplicate repeats were conducted in each orientation.

For cell morphological analysis, cell contour was identified by the stained actin. Cell morphology was then determined by using ImageJ software (National Institutes of Health, Bethesda, MD, USA), including cell projected area A, circularity ($4\pi A$/perimeter^2), and aspect ratio (long-axis length/short-axis length). 3D reconstruction along cell height was also conducted from sliced images for nucleus translocation analysis.

Cytoskeletal protein expression was analyzed by using relative fluorescence intensity or arbitrary unit values of stained actin, tubulin, or vimentin. To quantitatively compare these values for the 3 proteins in distinct orientations in repeated experiments, a calibration curve was conducted at systematically varied laser power and photomultiplier tube gain for the same fluorescent probes.

In the case of cytoskeletal protein inhibition, cells were incubated, respectively, with 50 ng/ml F-actin depolymizer cytochalasin D (Sigma-Aldrich) for 24 h, 150 nM tubulin polymerizing inhibitor nocodazole (Sigma-Aldrich) for 72 h, or 5 mM vimentin disrupting reagent acrylamide (Amresco, Solon, OH, USA) for an additional 6 h after the 72-h primary oriented culture. In the case of mechanotransductive signaling blockage, cells were incubated with Rho-associated protein kinase (ROCK) inhibitor Y-27632 (Cytoskeleton, Denver, CO, USA) at 5 μM for 24 or 72 h.

Cellular FAC rearrangement

FAC immunostaining protocol was similar to the aforementioned procedure for cytoskeleton staining. In brief, cells were corporately incubated with conjugated 5 μg/ml phalloidin, anti-paxillin mAbs (1:40), anti-vinculin mAbs (1:200), and anti–β1-integrin mAbs (1:100). After being incubated at 37°C for 60 min, cells were washed and then incubated with DyLight 594–labeled donkey anti-rabbit secondary Abs (1:200) for 60 min at 37°C. Collected cells were then rinsed and incubated with Hoechst 33342 for 10 min. FACs were visualized by using confocal microscopy by collecting 0.65-μm-thick information at the focal plane. The number of FACs per cell was counted for ≥60 cells total in each case. FAC size was estimated *via* MatLab software from confocal images with the following definitions: small focal complexes (FXs; 0.2–0.3 μm^2), intermediate focal adhesions (0.3–2.5 μm^2), and large super mature adhesions (SMAs; >2.5 μm^2), whereas those <0.2 μm^2 were neglected.

Phosphorylation of nuclear signaling molecules

Phosphorylation of nuclear lamin A/C was determined by using confocal microscopy. After cell fixation and permeation at 10 and 15 min, respectively, cells were rinsed and incubated in 1% bovine serum albumin/PBS for 60 min at 37°C to block nonspecific staining. Lamin A/C was incubated with anti–p-lamin A/C mAbs and stained with conjugated secondary Abs (5 μg/ml). After being incubated for 60 min at 37°C, cells were washed and incubated with Hoechst 33342 for 10 min to stain nuclei. Images of phosphorylated lamin A/C were examined. Triplicate repeats were conducted in each orientation.

DNA methylation by methylation-sensitive random amplified polymorphic DNA

Genomic DNA was isolated from cells placed at 180°, 0°, or 90° for 24 and 72 h using Mini BEST universal genomic DNA extraction kit, ver. 5.0 (Takara Bio, Kusatsu, Shiga, Japan) upon

manufacturer's instructions. Methylation-sensitive random amplified polymorphic DNA (RAPD) analysis of genomic DNA was performed as previously described (19). Four aliquots of 1 μg DNA were digested overnight at 37°C with 1 methylation insensitive restriction enzyme (Msp I) and 3 methylation sensitive restriction enzymes (Hpa II, Dpn I, and Dpn II), respectively. Restriction enzyme–digested as well as undigested genomic DNA was used for RAPD analysis. RAPD PCR amplifications were performed in 20 μl of reaction mixture that contained 10 μl of 2× Quick Taq HS DyeMix (Toyobo, Osaka, Japan), 100 nM of random primer (10 bp), and 25 ng of genomic DNA as template. Amplifications were performed in a DNA thermal cycler (Applied Biosystems, Foster City, CA, USA) programmed for 45 cycles: first cycle of 2 min at 94°C, 1 min at 34°C, and 2 min at 72°C; 44 cycles of 1 min at 94°C, 1 min at 34°C, and 2 min at 72°C, followed by a final extension cycle of 15 min at 72°C. PCR products were resolved on 1% agarose gel and detected by ethidium bromide.

Statistical analysis

D'Agostino-Person omnibus normality test was used if the values came from a Gaussian distribution. One-way ANOVA or Kruskal-Wallis test was performed to determine the statistical significance of differences among 3 orientations. Student's *t*-test or Mann-Whitney *U* test was also conducted when comparing the same parameter between 2 durations.

RESULTS

Cells reserve their mechanical and biological stabilities on orientated substrates

We first tested the morphology and function of cells placed at 180, 0, or 90° (Supplemental Fig. S1*A–F*). In an individual cell study, no significant differences were found for cell projected area, circularity, and aspect ratio in 3 orientations at 24 or 72 h (Supplemental Fig. S1*G–I*). Long-duration growth for up to 7 or 21 d in a confluent cell study does not induce remarkable alteration in cell cycle, proliferation, and osteogenic differentiation. Here, the percentage of G2/M, S, or G0/G1 phase was comparable at d 1, 3, and 7, respectively, among 3 orientations (Supplemental Fig. S1*J*). Similar ascending time course of cell proliferation was found for up to 7 d (Supplemental Fig. S1*K*). ALP activity induced by osteogenic-induced medium was relatively increased with time and reached saturation at d 21 in the same manner in 3 orientations (Supplemental Fig. S1*L*). These results indicated that the cells placed on differently orientated substrates can maintain their mechanical stability and biological homeostasis.

Nucleus translocation is deterministic and orientation dependent

A cell placed at 180, 0, or 90° could present differential translocation dynamics of the dense nucleus in cytosol. To elucidate whether such nucleus translocation is mediated by its Brownian motion, simple theoretical analysis was conducted by estimating a dimensionless parameter $G_T = \Delta\rho V g d / k_B T$ between gravity potential and thermal energy scale. By using typical values of these parameters: $\Delta\rho \sim 0.3$ g/cm^3 (20, 21), $V \sim 500$ μm^3 (22), $g \sim 10$ m/s^2, $d \sim 10$ μm (23), $k_B = 1.38 \times 10^{-23}$ J/K, $T \sim 300$ K, and G_T r$O(10^3) >> 1$. This analysis suggested that nucleus translocation is a deterministic process that is mediated by gravity vector–directed effects but is not attributed to random Brownian fluctuation.

To test this experimentally, nucleus longitudinal height—defined as the distance from nucleus centroid to the bottom surface of substrate (Fig. 1*A*, *B*)—is used to measure the capability of nucleus translocation as it could exclude the potential impact of cell deformation or spreading on absolute nucleus translocation. Typically, it reads approximately one-half of cell height (~3.2–4.8 μm) with less scattered distribution (Fig. 1*C*). We further compared those values in 3 orientations at 2 time points. At 24 h, the height yields were at a significantly higher median value at 0° (1.71 μm) compared with that at 180° (1.54 μm) or at 90° (1.53 μm). By contrast, it presents at 72 h a distinct pattern, with the higher value at 90° (1.64 μm) compared with that at 180° (1.41 μm) or at 0° (1.45 μm; Fig. 1*C*), which implies that orientation dependence of nucleus longitudinal translocation is presented in distinct patterns at short or long duration. Further comparison between 24 and 72 h indicated that the height is reduced with time at 180 or 0° but is slighted enhanced at 90° without significant differences. These results indicated that distinct orientation dependence of nucleus longitudinal translocation is presented in the pattern of low-high-low at 24 h or low-low-high at 72 h for upward-downward-edge on orientation. Moreover, from 24 to 72 h, nucleus longitudinal translocation could be slowed down consistently to the substrate at 180° or be restored to the substrate at 0°, whereas it keeps steady at 90°.

We also compared 2 other types of nucleus translocation. On one hand, nucleus lateral translocation on the *x-y* plane was present at a typical median value of ~5 μm (varying from 0 to 20 μm) in an indifferent manner in 3 orientations (Supplemental Fig. S2A). Because a spread cell covers ~50 μm in its equivalent diameter, the lateral translocation is only ~1/10 of cell scale. On the other hand, relative nucleus translocation along a gravity vector in edge-on orientation yielded a median value of −1.35 μm at 24 h and −0.20 μm at 72 h (*i.e.*, fluctuating around 0; Supplemental Fig. S2B). Noting that the positive or negative value at 24 or 72 h at 90° represents the net translocation along with or opposite to a gravity vector from cell centroid, these results implied that gravity vector–directed nucleus migration should not be necessarily aligned along the vector at 90°. Combined with nucleus translocation in upward or downward orientation along with or opposite to the vector, nucleus longitudinal height could serve as a primary indicator of nucleus translocation.

Directed nucleus translocation is mechanically balanced by cytoskeletal remodeling

Mechanical stability of nucleus translocation is achieved by balancing the net force of nucleus weight minus buoyant force with mechanical forces exerted by

cytoskeletal network. Here, we focused on nucleus longitudinal height because it is able to probe the mechanical balance under a gravity vector. We first compared the expressions of actin, vimentin, and tubulin within an entire cell. At 24 h, actin (**Fig. 2*A***) or vimentin (Fig. 2*B*) expression is higher at 0° than at 180 or 90°, which is consistent with the orientation dependence of nucleus longitudinal height at same time (*cf.*, Fig. 1*C*), whereas tubulin expression is comparable among 3 orientations (Fig. 2*C*). At 72 h, vimentin or tubulin expression is relatively higher at 90° than at 180° or 0° (Fig. 2*B*, *C*), which is also in accordance with the orientation dependence of the height at the same time. Moreover, orientation dependence of actin expression at 24 h is amplified at 72 h, yielding the highest value at 0° (Fig. 2*A*). These data suggested that cytoskeletal remodeling presents similar orientation dependence for actin and vimentin at 24 h and for vimentin and tubulin at 72 h, which supports the mechanical stability of nucleus in cytosol.

In addition to orientation-dependent global expression of cytoskeletal proteins, the reorganized pattern of these proteins at the periphery of the nucleus also plays a critical role in maintaining the mechanical stability of the nucleus. Perinuclear actin stress fiber (Fig. 2*D*) and vimentin cord (Fig. 2*F*) were measured for comparison. On one hand, the collected number of stress fibers across the nucleus or actin cap (24, 25) follows the same orientation dependence as global actin expression at both 24 and 72 h (*i.e.*, higher value at 0° than at 180 or 90°; Fig. 2*E*, left), which yields the same orientation-dependent pattern as nucleus longitudinal height at 24 h (Fig. 1*C*) but is a different pattern at 72 h where stress fiber no longer presents the highest number at 90°. On the other hand, vimentin tends to form a cord-like structure to surround or support the nucleus, and vimentin cord number manifests as a similar (at 24 h) or identical (at 72 h) orientation dependence with nucleus longitudinal height (Fig. 2*E*, right). Moreover, higher vimentin cord number at 90° at 72 h is dominant for mechanically supporting the cell placed perpendicular to the substrate where stress fiber number is relatively low (Fig. 2*E*). In addition, these findings were also supported by actin expression along either long or short axis of nuclear periphery where the same orientation dependencies were presented at 24 or 72 h (Supplemental Fig. S3*A*–*C*) or by similar orientation-dependent distribution of small- and large-sized cords except for an orientation-independent distribution of large cords at 24 h (Supplemental Fig. S3*D*, *E*). Taken together, orientation dependence of nucleus longitudinal height is positively correlated with perinuclear remodeling of actin and vimentin, which supports nuclear mechanical stability.

Reorganized cytoskeleton is mechanically linked to FACs

FACs are major mechanical elements that connect the intracellular cytoskeletal network to the substrate. We tested the orientation dependence of FACs depicted as colocalized actin, vinculin, paxillin, and β1-integrin (**Fig. 3*A***). At 24 h, total FAC area, which defines anchorage strength

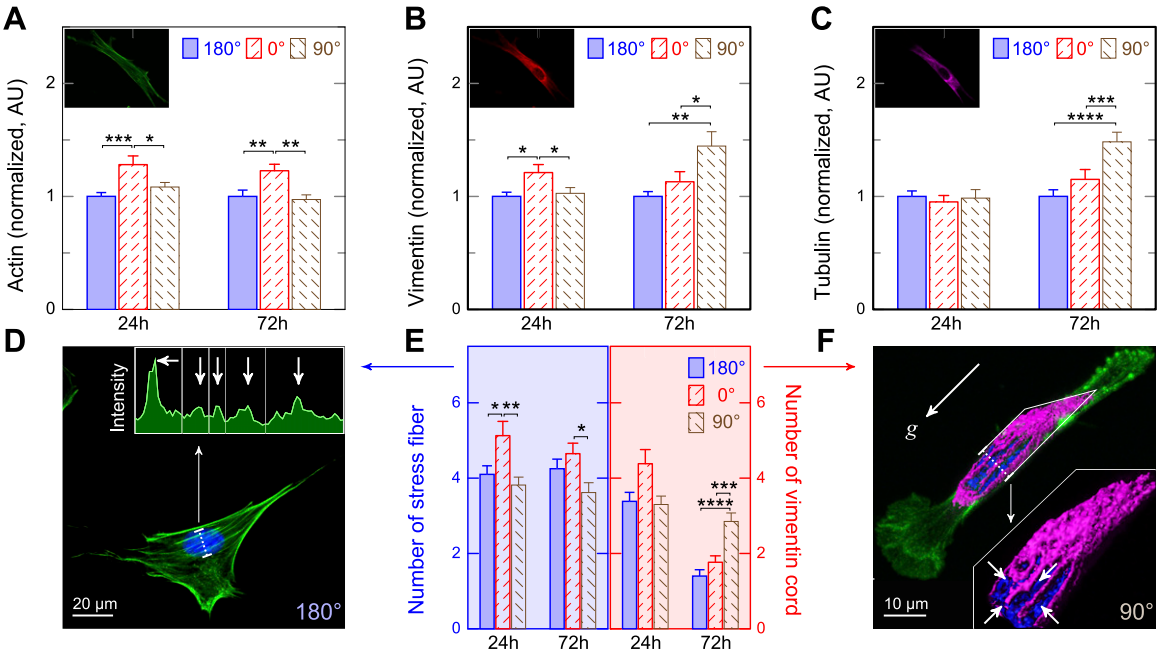

Figure 2. Expressions and structures of cytoskeletal proteins in 3 orientations. *A*–*C*) Actin (*A*) vimentin (*B*) or tubulin (*C*) expression is illustrated in respective inserts. Measured intensity is normalized to the those at 180° and presented as means ± SE of 60 cells from 3 experiments. *D*, *F*) Typical images are presented for defining the perinuclear actin stress fiber (*D*; at 180° at 72 h, line indicates the position for measurement and arrows in the insert denote stress fibers) and the vimentin cord (*F*; at 90° at 24 h, arrows indicate vimentin cords). *E*) Measured numbers of perinuclear stress fiber (left) and vimentin cord (right) are presented as means ± SE of 60 cells from 3 experiments. Au, arbitrary unit. $^{*}P < 0.05$; $^{**}P < 0.01$; $^{***}P < 0.001$; $^{***}P < 0.0001$.

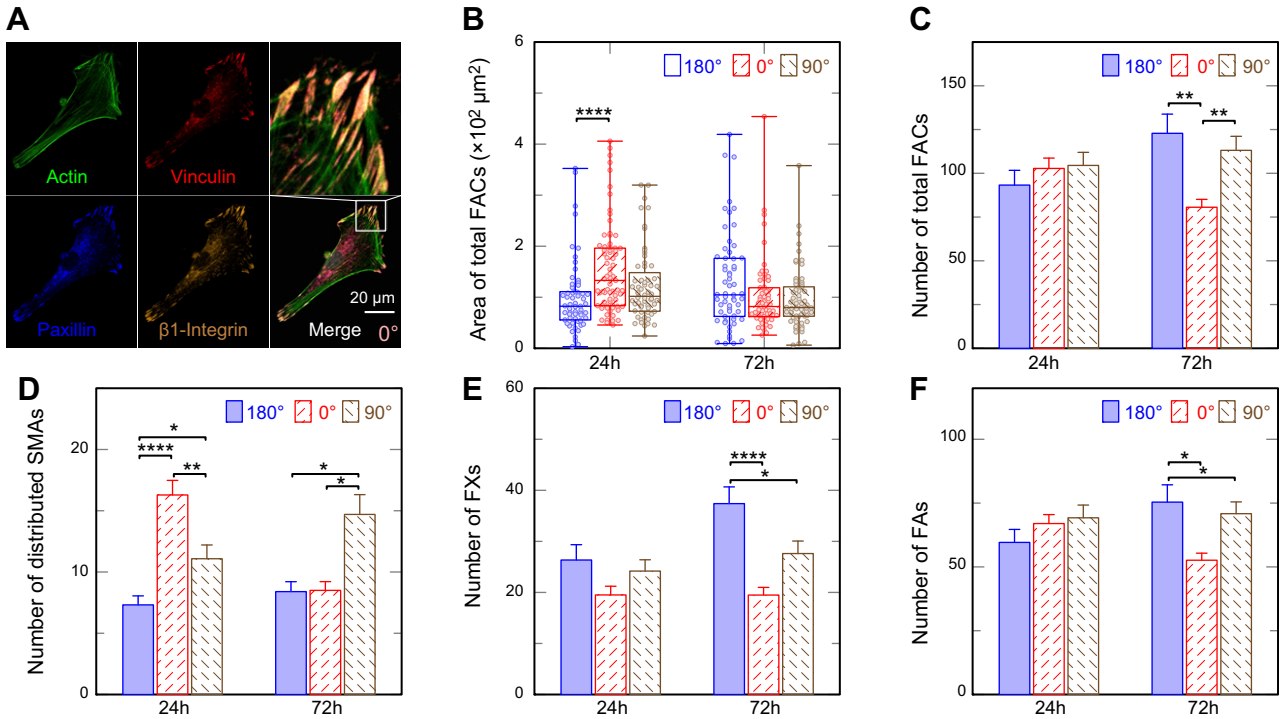

Figure 3. Distribution of FACs in 3 orientations. *A*) A typical image is plotted with costained actin (green), vinculin (red), paxillin (blue), and β1-integrin (orange) at 0° at 24 h. *B–F*) Also plotted are the distributions of total FAC area (*B*; presented as median values with 25 and 75th percentiles) as well as the numbers of total FACs (*C*) SMAs, (*D*) FXs, (*E*) or focal adhesions [FAs (*F*); presented as means ± SE] of 60–76 cells from 2 or 3 experiments. $*P < 0.05$; $**P < 0.01$; $****P < 0.0001$.

between the cell and the substrate, is relatively higher at 0° than at 180° or 90° (Fig. 3*B*), which is consistent with orientation dependence of nucleus longitudinal translocation. In contrast, no orientation dependence was found at 72 h (Fig. 3*B*). These results suggest that FAC area is presented in an orientation-dependent pattern at short duration and becomes similar among the 3 orientations at long duration.

In addition, we tested the number distribution of differently sized FACs in 3 orientations (26, 27). Total FAC number is presented as the mean value of ~80–120 per cell. No orientation dependence was seen in total FAC number at 24 h, whereas the number at 0° is significantly lower than 180 or 90° at 72 h (Fig. 3*C*). This observation suggests that FACs could be made to disassemble at 0° at long duration as a result of the persistent action of a gravity vector (28). Even in this case, the cell is mechanically stable as its anchorage strength is determined by total FAC area with similar values at 180 or 90° (Fig. 3*B*). Noting that large-sized SMAs provide major mechanical support for cell anchorage (29), we further compared the orientation dependence of SMA presentation and found that SMA number follows similar orientation dependence as nucleus longitudinal translocation at 24 or 72 h (Fig. 3*D*). By contrast, the summation of small-sized FXs and intermediately sized FAs yields the majority (>70%) of total FAC number but presents distinct patterns among the 3 orientations (Fig. 3*E*, *F*). Collectively, these results imply that FAC area and SMA number play dominant roles in regulating cell stability and present similar orientation dependence as nucleus longitudinal translocation at least at short duration.

Intranuclear response is correlated to gravity vector–directed nucleus translocation

Intracellular reorganization and signaling pathway finally induces intranuclear events to rebuild the mechanical stability and biological homeostasis from altered gravity vector and to implement their biological functions. We investigated the orientation-directed phosphorylation of a typical nuclear lamina protein, lamin A/C. Ser^{22} phosphorylation of lamin A/C yielded similar intensity in 3 orientations at 24 h but presented as a higher value at 0 or 90° compared with 180° at 72 h, which implies the correlation of lamin A/C phosphorylation with oriented substrate at long duration (**Fig. 4*A***). Whereas the orientation dependence of Ser^{22} phosphorylation was not identical to that of nucleus longitudinal height at 72 h, it was consistent with that of side-viewed perinuclear actin expression (Supplemental Fig. S3*A–C*) and presented the same highest value at 90° for perinuclear vimentin expression (Fig. 2*B*, *E*). We further analyzed the morphological alteration of the nucleus. At 24 h, the cell nucleus preserves the stable shape in 3 orientations with similar projected area and cell height; however, at 72 h, the nucleus at 0° tends to further spread with enhanced projected area and reduced height compared with 180 or 90° (Fig. 4*B*, *C*). Taken together, orientated substrate induces distinct intranuclear phosphorylation of a mechanosensitive molecule and mediates nucleus spreading in an orientation-dependent manner at long duration.

One more possible mechanism for intranuclear responses to gravity vector–directed nucleus translocation

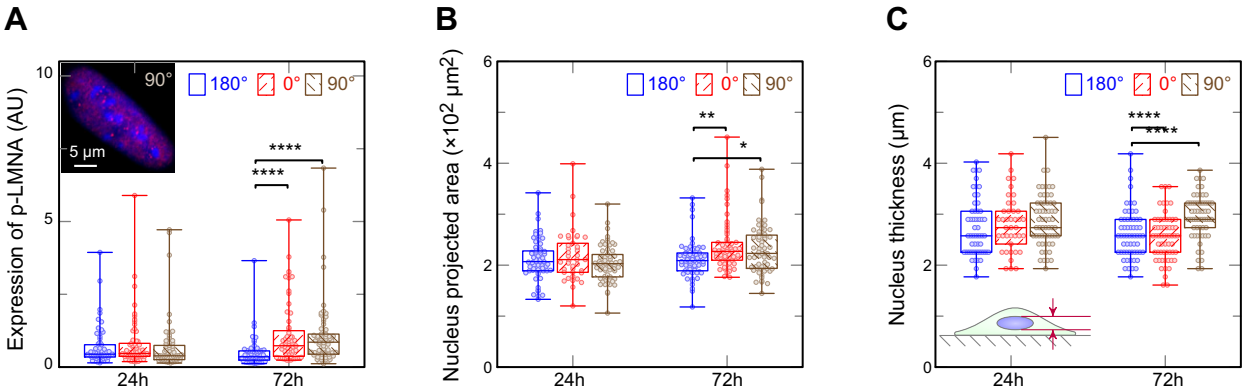

Figure 4. Nuclear cytoskeletal protein phosphorylation and nucleus morphology in 3 orientations. *A*) A typical image is illustrated for phosphorylated Ser22 residue of lamin A/C (red) at 0° at 24 h (insert) and measured intensity is presented as median values with 25 and 75th percentiles of 60 cells from 3 experiments. *B*, *C*) Also plotted are the projected area (*B*) and thickness (*C*) of the nucleus for 40–60 cells from 3 experiments. Au, arbitrary unit; LMNA, Lamin A/C. $*P < 0.05$; $**P < 0.01$; $****P < 0.0001$.

may be attributed to its epigenetic response. Here, we simply tested DNA methylation in 3 orientations at 24 or 72 h by using methylation-sensitive RAPD fingerprinting analysis. Data indicated that none of 9 random primers used presented any significant changes in DNA fingerprints (Supplemental Fig. S4), which suggested that, at the least, DNA methylation recognized by 3 sensitive restriction enzymes (Hpa II, Dpn I, and Dpn II) cannot serve as the signaling candidates in mechanoepigenetic responses to orientated substrate.

Cytoskeleton is critical for regulating nucleus translocation and FAC rearrangement

From the above observations, we proposed that gravity-directed sedimentation of dense nucleus in cytosol could be balanced by cytoskeletal remodeling around nucleus in an orientation-dependent pattern, which initiates the redistribution of FACs locating around the cell membrane to achieve mechanical stability. To validate the hypothesis, we applied the respective inhibitors of actin, tubulin, and vimentin to disrupt the cytoskeletal network, and the data measured from treated cells were normalized by their respective values from intact cells (**Fig. 5*A*–*C***). Nucleus longitudinal height was relatively reduced, and original orientation dependence of nucleus longitudinal translocation was diminished in cells treated with cytochalasin D for 24 h (Fig. 5*A*′), with nocodazole for 72 h (Fig. 5*B*′), or with acrylamide for an additional 6 h after 72 h of growth (Fig. 5*C*′). Moreover, cytochalasin D treatment reduced FAC area (Fig. 5*A*′′) or number (Supplemental Fig. S5*A*), and orientation dependences of FAC area and SMA number were no longer observed. Of interest, the reduced SMA and enhanced FX fractions implied that actin depolymerization could fragment large SMAs into small FXs (Supplemental Fig. S5*A*). Nocodazole treatment lowered FAC area or number, and no orientation dependences of FAC area and SMA number were observed (Fig. 5*B*′′ and Supplemental Fig. S5*B*). Specifically, the area and the number were dramatically reduced at 0°, mainly as a result of positive correlation of tubulin expression with FAC formation (see Fig. 3*C*) (30, 31). Additional acrylamide treatment significantly enhanced FAC area or number and resulted in the much higher value at 0° (Fig. 5*C*′′ and Supplemental Fig. S5*C*). Here, orientation dependence of total FAC number was reversed compared with that for intact cells (Fig. 3*C*). Collectively, cytoskeletal depolymerization diminishes the orientation dependence of nucleus longitudinal translocation together with distinct FAC distributions in 3 orientations.

Mechanosensitive ROCK signaling is prominent in maintaining biological homeostasis

ROCK signaling is a well-known pathway in mechanotransduction, which converts mechanical signals into biochemical signaling. We repeated the above tests by adding ROCK inhibitor Y-27632 to induce cell remodeling (**Fig. 6*A***). Nucleus longitudinal height was relatively enhanced, and original orientation dependence of nucleus longitudinal translocation was attenuated at 24 h and finally diminished at 72 h (Fig. 6*B*). Comparable value of nucleus lateral translocation or relative nucleus translocation along a gravity vector at 24 or 72 h also presented similar orientation indifference (data not shown). FAC area was reduced significantly at 0 or 90° at 24 or 72 h, and original orientation dependence of FAC area for intact cells was attenuated at 24 h and finally diminished at 72 h (Fig. 6*C*). This is presumably attributed to the reduced FAC area by ROCK inhibition and the forced dissociation of FAC, especially at 0 or 90°. In addition, no morphological change of treated cells was found, except for slightly enhanced circularity at 24 or 72 h compared with intact cells, which yielded similar orientation independence (Supplemental Fig. S6*A*–*C*). Fractionalized FAC numbers were reduced significantly at 0 or 90° at 24 or 72 h (Supplemental Fig. S6*D*).

We also compared expressions of cytoskeletal proteins as one critical role of ROCK signaling is to regulate cytoskeletal network. At 24 h, actin expression (Fig. 6*D*) was significantly reduced but the same orientation dependence

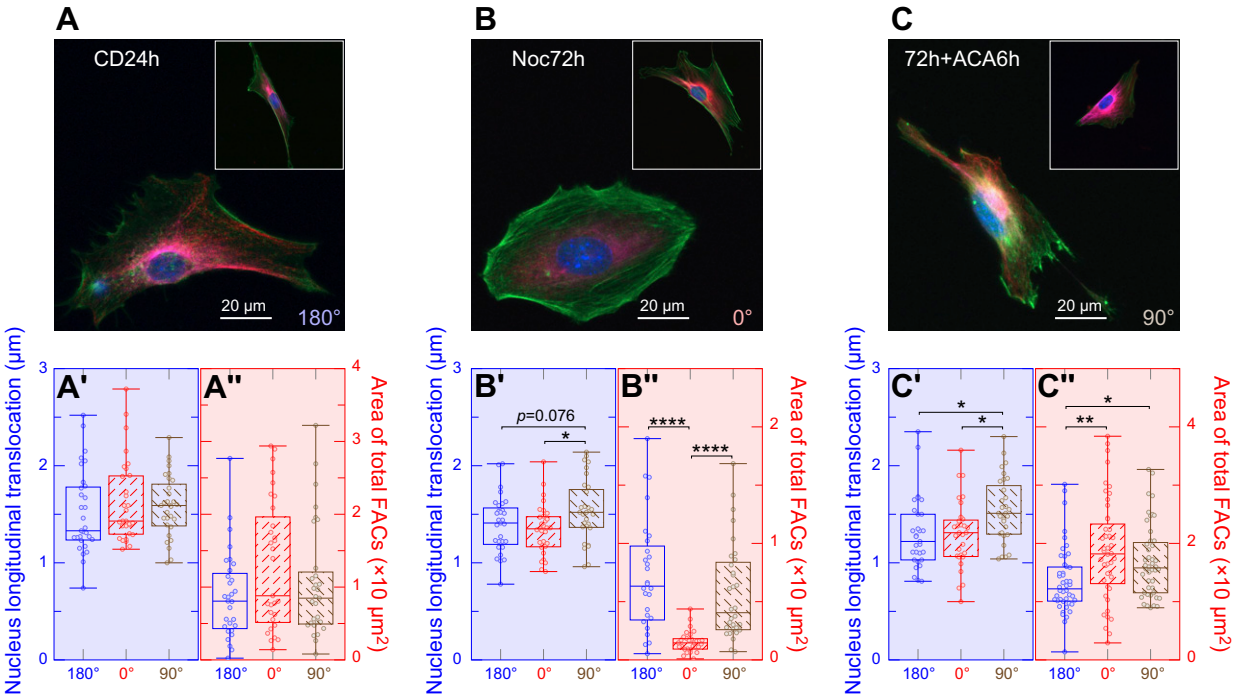

Figure 5. Disruption of cytoskeletal network in 3 orientations. *A–C*) Typical images are illustrated for actin depolymerization *via* cytochalasin D at 180° at 24 h (*A*) tubulin polymerization inhibition *via* nocodazole at 0° at 72 h (*B*) or vimentin collapse *via* incubating cells with acrylamide for an additional 6 h after 72 h of primary culture at 90° (*C*). Three proteins are stained with same colors as those in Fig. 3 and the insert in each panel denotes respective typical image of an intact cell. Data are presented as median values with 25 and 75th percentiles for nucleus longitudinal height (*A′–C′*) and total FAC area (*A′′–C′′*) of 30–45 cells from 2 experiments. $*P < 0.05$; $**P < 0.01$; $****P < 0.0001$.

was retained. Vimentin expression was lower and presented distinct orientation dependence with a higher value at 180° (Fig. 6*E*). Tubulin expression was enhanced (Fig. 6*F*) and retained the same orientation dependence. At 72 h, actin, tubulin, or vimentin expression was further reduced (Fig. 6*D–F*) but retained similar orientation dependence. Therefore, ROCK pathway inhibition diminished those orientation dependences of nucleus longitudinal height and FAC area in 3 orientations, whereas the dependences of cytoskeletal protein expression are most likely unaltered.

DISCUSSION

This work aims to elucidate how a normal-sized mammalian cell could rebuild its mechanical stability from altered gravity vector and then possess its biological function under gravity vector. Our data demonstrate that orientation dependence of nucleus longitudinal translocation is positively correlated with cytoskeletal remodeling of their expressions and structures and is associated with rearrangement of FAC. Theoretical analysis was also conducted to decipher the mechanical stability of a cell on an oriented substrate, and a biomechanical model is proposed on the basis of a simplified configuration of a cell (**Fig. 7*A***). At 180°, the nucleus tends to migrate toward the substrate. Microtubule and vimentin are reorganized to resist nucleus translocation, and compression of microtubule reduces nucleus spreading. Nucleus translocation reduces tension of actin, which leads to enhancement of FAC area (Fig. 7*B*). At 0°, the nucleus tends to migrate away from the substrate. Actin is reorganized to resist nucleus translocation, and tension of microtubule enhances nucleus spreading. Nucleus translocation enhances tension of actin, which leads to the reduction of FAC area (Fig. 7*C*). At 90°, the nucleus attempts to migrate away from the substrate mainly because compression of microtubule prevents—*via* enhanced vimentin expression and cord formation—nucleus migration along gravity vector. Tension of actin provides resistant torque to impede persistent longitudinal translocation of nucleus. Unevenly distributed actin fibers also enhance nucleus spreading to a lesser extent but reduce total FAC area (Fig. 7*D*, *E*). Major components of cytoskeletal network inside a cell are illustrated (Fig. 7*F*). This model is able to predict the gravisensing mechanisms on orientated substrate. As exemplified for cells placed at 0° at long duration, higher actin tension, presented as enhanced actin expression and stress fiber number (Fig. 2*A*, *D*), pulls apart the nucleus symmetrically and then fosters cell and nucleus spreading (Supplemental Fig. S1*H* and Fig. 4*B*, *C*). By contrast, it also pulls down existing FACs and reduces FAC number (Fig. 3*C*), which implies a negative correlation of nucleus area with FAC number. Combination of these observations with the proposed model (Fig. 7*C*) could suggest why the nucleus tends to spring back with reduced longitudinal height at long duration (Fig. 1*B*).

Gravity-induced translocation of the dense nucleus is the primary mediator for cell remodeling. For cells placed on differently orientated substrate, early studies have

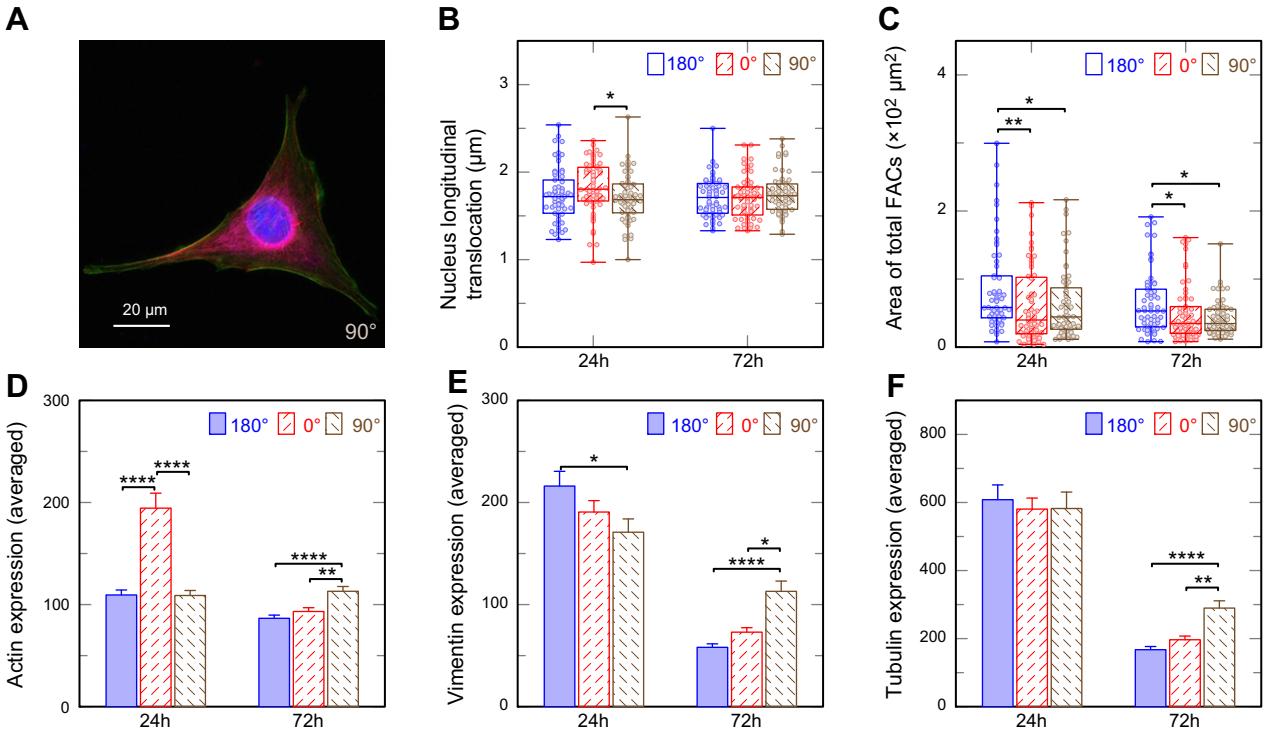

Figure 6. Inhibition of ROCK pathway *via* Y-27632 inhibitor in 3 orientations. *A*) A typical image is illustrated for a cell at 90° at 72 h using same colors as those in Fig. 3. *B–F*) Data were presented as median values with 25 and 75th percentiles for nucleus longitudinal height (*B*) or total FAC area, (*C*) or as means ± SE for actin, (*D*) vimentin, (*E*) or tubulin, (*F*) expression of 60 cells from 3 experiments. $*P < 0.05$; $**P < 0.01$; $****P < 0.0001$.

reported the existence of high-density nuclear structures (32, 33) that attempt to relocate toward the apical surface or basolateral membrane and, in turn, apply extra forces on the cytoskeletal fibers adjacent to the nucleus. Recent evidence indicates that, after complete nucleus flattening, apparent nucleus height is significantly reduced significantly to a value of ~3 μm, and the gap between the top cell surface and the top nuclear surface approaches zero, in which at least microtubules, intermediate filaments, and linker of nucleoskeleton and cytoskeleton complex are all dispensable (34). Those observations are consistent with our data that demonstrates nucleus longitudinal height and dominant distribution of actin and tubulin in the space between substrate and nucleus at 180°. Meanwhile, cell nucleus or nucleolus is assumed to present liquid-like behaviors, presumably with viscoelastic nature (35, 36). Regardless of a very small density difference between nucleus and cytosol, nucleus translocation is directed by gravitational force rather than by thermal fluctuation. This process appears not only in a large-sized oocyte cell (6), but also in a normal-sized mammalian cell in the current work, with similar criteria of limited sedimentation length for the former or of 3-order lower energy of Brownian motion for the latter. Moreover, time courses of nucleus translocation are differential in distinct orientations (Fig. 1 and Supplemental Fig. S2). It is also noted that cell height at $1 \times g$ is reduced when comparing cells placed in downward orientation with those in upward orientation (data not shown), which is qualitatively consistent with the previous observation of a whole-cell height decrease when the same type of cell is exposed to hypergravity at 2 or 3 *g* (37). Our work has special significance for cell gravisensing on Earth by the long-term accumulation of gravity vector–directed effects, as it overturns the conventional viewpoint that the gravity of a normal-sized mammalian cell is too small to mediate direct cell mechanosensing.

Cytoskeletal network remodeling is critical for maintaining mechanical stability and implementing the biological function of cells that are exposed to gravity. In cell meiosis, microtubules can also drive the nuclear rotation, mainly *via* SUN (Sad1p, UNC-84) at the nuclear envelope (38). Compression-resisted microtubules are ductile materials with a self-healing feature and lattice plasticity, which enables the adaptation of microtubules to mechanical stress *via* forced softening or stiffening (39). Presence of vimentin, lamin A/C, and SUN-domain protein linkage, but not F-actin or microtubules, is required for a stiff, elastic response of the nucleus to sudden suction or relaxation in fast dynamics (a few seconds), which indicates that intermediate filament networks maintain nuclear mechanical stability against localized forces (40). In conventional cell attachment at 180°, the denser nucleus settles down to the bottom and the interconnected cytoskeleton maintains the nucleus in place. By contrast, at 0 or 90°, the nucleus is relocated toward the apical surface or basolateral membrane and pulls down the cytoskeletal network inside the cell. More importantly, perinuclear distribution of cytoskeletal proteins promotes formation of the orientation-dependent actin stress fiber with consistent actin expression along the long or short axis of the nucleus

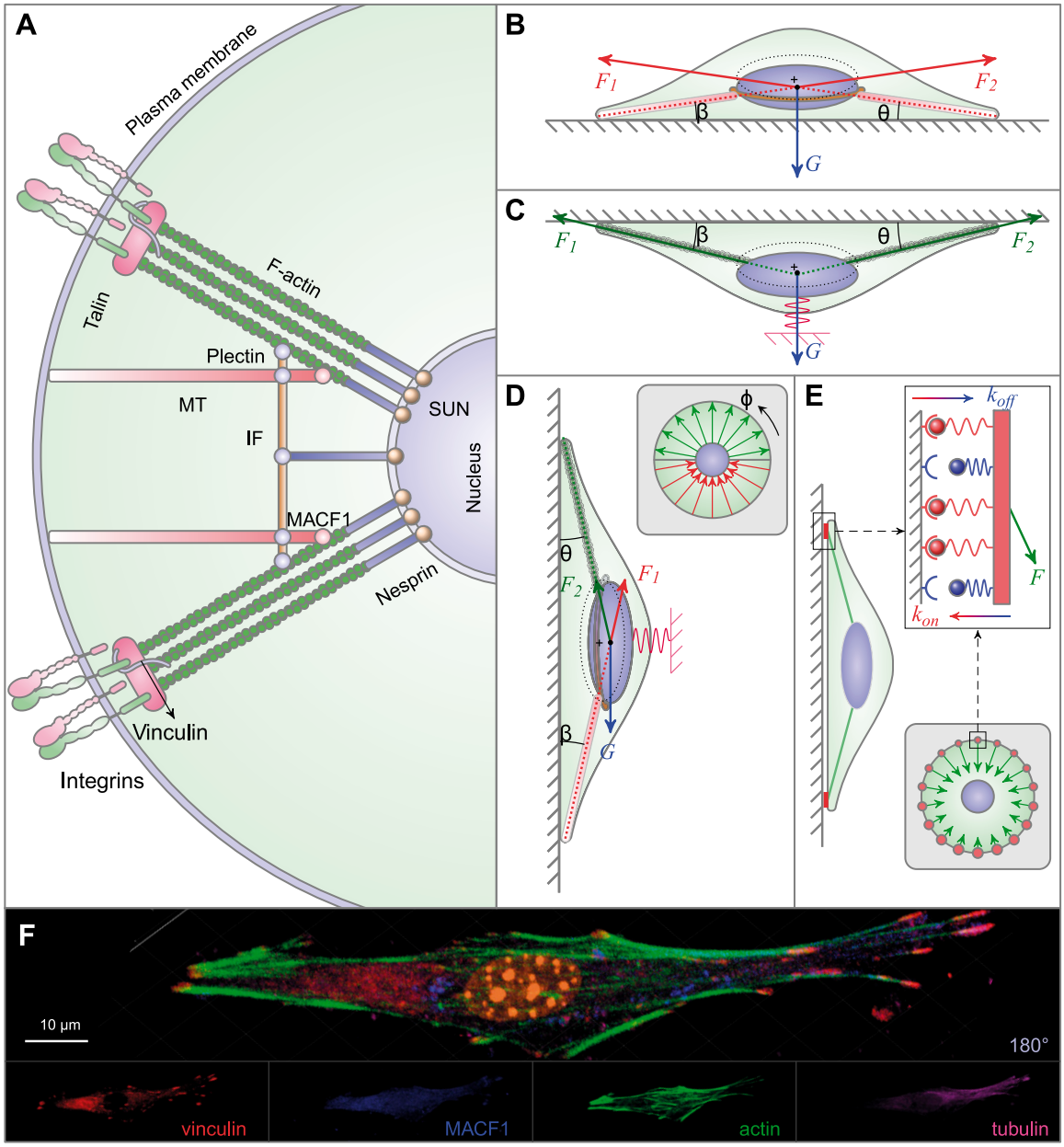

Figure 7. Working model of gravity-directed responses for a mammalian cell in oriented substrate. *A*) Mechanical stability of dense nucleus is supported by cytoskeletal network. *B–D*) Mechanical forces exerted on the nucleus are balanced differentially in upward, (*B*) downward, (*C*) or edge-on orientation, (*D*) by tension-resistant actin, compression-resistant tubulin, and connecting vimentin. *E*) Typical force analysis is illustrated in edge-on orientation. *F*) Also plotted is a 3D image for a cell with costained vinculin (red), MACF1 (Microtubule-actin cross-linking factor 1 blue), actin (green), and tubulin (magenta) to demonstrate the underlying mechanosensing pathway. IF, intermediate filament; MT, microtubule; SUN, Sad1p, UNC-84.

or to visualize vimentin cord with similar orientation dependence of nucleus longitudinal translocation (Fig. 2), in which these specialized perinuclear structures are able to resist nucleus translocation. This observation is supported by the fact that blockage of actin, tubulin, or vimentin diminishes orientation dependence of nucleus longitudinal translocation (Fig. 5 and Supplemental Fig. S5). Meanwhile, ROCK inhibition significantly reduces expression of actin, tubulin, and vimentin in 3 orientations (Fig. 6 and Supplemental Fig. S6), as ROCK is placed at the hub of the complex signaling network that controls actomyosin contractility and stress fiber assembly (41). Noting that the specialized structures of actin stress fiber and vimentin cord are also visualized for Ros 17/2.8 cells placed in the 3 orientations at 120 h (5), these results imply the universality of these structures for biodiverse cell models.

Anchorage of a cell on substrate requires point-attached FACs to provide mechanical support. These FACs undergo rearrangement when the cell is placed on orientated substrate. Inside FAC, talin diagonally spans the focal adhsion core with its N terminus attached at the membrane with ~15° and C terminus demarcating the focal adhesion/stress fiber interface, whereas vinculin is dispensable for specification of focal adhesion nanoscale

architecture (42). Assuming that mean force per unit FAC area is approximately 1 ± 0.2 nN/μm^2 (29), cell adhesive force with total ~100 μm^2 FAC area (Fig. 3*B*) presents as ~100 nN, which is 5 orders of magnitude higher than cell weight (~1 pN) to sufficiently support the cell. Moreover, blockage of actin or tubulin significantly reduces FAC area or distinctly sized number. An exceptional case comes from the blockage of vimentin at 0°, where FAC area or number is almost doubled, which results in enhanced FAC strength for supplementing the reduced mechanical support originated from vimentin cord at long duration. In addition, ROCK inhibition remarkably reduced FAC area but had little impact on FAC number, even though assembly of FACs is triggered by ROCK signaling (8).

All the events of nucleus translocation, cytoskeletal remodeling, and FAC rearrangement could finally induce intranuclear epigenetic responses as nucleus deformation, skeletal protein reorganization, and epigenetic alteration could serve as typical indicators for cell mechanoepigenetics. The cell nucleus tends to deform when responding to intracellular (cytoskeletal prestress) or extracellular forces (shear, tension, or compression) or when sensing the surrounding physical microenvironment, such as substrate stiffness or microtopography (35, 43). When a cell spreads in fast dynamics (≤120 min), the basal-to-apical polarization of the nuclear envelope appears on differential epitope accessibility of the nuclear skeletal protein lamin A (44). Moreover, lamin A/C complex directs the mitotic spindle assembly in a microtubule- and actin-dependent manner (45), which confirms the critical role of lamin proteins in the mechanical connection between cortex membrane and nuclear envelope. Whereas biochemically induced phosphorylation is a fast, transient process, it is also reasonable to assume that lamin A/C phosphorylation mediated by persistent mechanical stimulus could last a long time, as observed in cells on soft or stiff gels that show different lamin A phosphorylation for several days culture (44). We present here the increased Ser^{22} phosphorylation of lamin A/C complex at 0 or 90° at long duration, together with correspondingly enhanced nucleus area (Fig. 4). No significant alteration in cell morphology implies that the intranuclear responses could finally support the mechanical stability of the cell placed differently.

CONCLUSIONS

Sedimentation of the dense nucleus tends to compress the basolateral membrane and stretch the apical membrane along the gravity vector when the cell is placed in upward orientation. The opposite occurs when the cell is placed in downward orientation. It seems not to induce asymmetric responses for the upper and lower regions of a cell when placed in edge-on orientation. Such an intracellular mechanical alteration should be balanced by internal traction forces that originate from remodeling of cytoskeletal proteins distributed in distinct zones within the cell, which results in similar orientation dependence of nucleus translocation. Eventually, mechanical stability of the entire cell is achieved by linking intracellular elements to extracellular substrate *via* rearranging FACs. FJ

ACKNOWLEDGMENTS

The authors thank Dr. Yan Zhang (Institute of Mechanics, Chinese Academy of Sciences), for technical assistance. This work was supported by National Key Basic Research Foundation of China Grant 2011CB710904, Strategic Priority Research Program Grants XDA04020219 and XDA01030102, National Natural Science Foundation of China Grant 31110103918, and National High Technology Research and Development Program of China Grant 2011AA020109.

AUTHOR CONTRIBUTIONS

C. Zhang, D. Lü, S. Sun, and M. Long designed the research; C. Zhang, L. Zhou, F. Zhang, N. Li, L. Zheng, Y. Xu, and Z. Li performed the research and the modeling; C. Zhang, L. Zhou, F. Zhang, N. Li, and L. Zheng analyzed the data; and C. Zhang, L. Zhou, and M. Long wrote the paper.

REFERENCES

1. Morita, M. T. (2010) Directional gravity sensing in gravitropism. *Annu. Rev. Plant Biol.* **61**, 705–720
2. Vassy, J., Portet, S., Beil, M., Millot, G., Fauvel-Lafève, F., Karniguian, A., Gasset, G., Irinopoulou, T., Calvo, F., Rigaut, J. P., and Schoevaert, D. (2001) The effect of weightlessness on cytoskeleton architecture and proliferation of human breast cancer cell line MCF-7. *FASEB J.* **15**, 1104–1106
3. Helmstetter, C. E. (1997) Gravity and the orientation of cell division. *Proc. Natl. Acad. Sci. USA* **94**, 10195–10198
4. Kacena, M. A., Todd, P., Gerstenfeld, L. C., and Landis, W. J. (2002) Experiments with osteoblasts cultured under varying orientations with respect to the gravity vector. *Cytotechnology* **39**, 147–154
5. Li, H., Chen, J., Zhang, Y., Sun, S., Tao, Z., and Long, M. (2010) Effects of oriented substrates on cell morphology, the cell cycle, and the cytoskeleton in Ros 17/2.8 cells. *Sci. China Life Sci.* **53**, 1085–1091
6. Feric, M., and Brangwynne, C. P. (2013) A nuclear F-actin scaffold stabilizes ribonucleoprotein droplets against gravity in large cells. *Nat. Cell Biol.* **15**, 1253–1259
7. Ulbrich, C., Pietsch, J., Grosse, J., Wehland, M., Schulz, H., Saar, K., Hübner, N., Hauslage, J., Hemmersbach, R., Braun, M., van Loon, J., Vagt, N., Egli, M., Richter, P., Einspanier, R., Sharbati, S., Baltz, T., Infanger, M., Ma, X., and Grimm, D. (2011) Differential gene regulation under altered gravity conditions in follicular thyroid cancer cells: relationship between the extracellular matrix and the cytoskeleton. *Cell. Physiol. Biochem.* **28**, 185–198
8. Bershadsky, A. D., Ballestrem, C., Carramusa, L., Zilberman, Y., Gilquin, B., Khochbin, S., Alexandrova, A. Y., Verkhovsky, A. B., Shemesh, T., and Kozlov, M. M. (2006) Assembly and mechanosensory function of focal adhesions: experiments and models. *Eur. J. Cell Biol.* **85**, 165–173
9. Meloni, M. A., Galleri, G., Pani, G., Saba, A., Pippia, P., and Cogoli-Greuter, M. (2011) Space flight affects motility and cytoskeletal structures in human monocyte cell line J-111. *Cytoskeleton (Hoboken)* **68**, 125–137
10. Franz, C. M., and Müller, D. J. (2005) Analyzing focal adhesion structure by atomic force microscopy. *J. Cell Sci.* **118**, 5315–5323
11. Kanchanawong, P., Shtengel, G., Pasapera, A. M., Ramko, E. B., Davidson, M. W., Hess, H. F., and Waterman, C. M. (2010) Nanoscale architecture of integrin-based cell adhesions. *Nature* **468**, 580–584
12. Humphries, J. D., Wang, P., Streuli, C., Geiger, B., Humphries, M. J., and Ballestrem, C. (2007) Vinculin controls focal adhesion formation by direct interactions with talin and actin. *J. Cell Biol.* **179**, 1043–1057
13. Guignandon, A., Usson, Y., Laroche, N., Lafage-Proust, M. H., Sabido, O., Alexandre, C., and Vico, L. (1997) Effects of intermittent or continuous gravitational stresses on cell-matrix adhesion: quantitative analysis of focal contacts in osteoblastic ROS 17/2.8 cells. *Exp. Cell Res.* **236**, 66–75
14. Del Rio, A., Perez-Jimenez, R., Liu, R., Roca-Cusachs, P., Fernandez, J. M., and Sheetz, M. P. (2009) Stretching single talin rod molecules activates vinculin binding. *Science* **323**, 638–641

15. Hoffman, B. D., Grashoff, C., and Schwartz, M. A. (2011) Dynamic molecular processes mediate cellular mechanotransduction. *Nature* **475**, 316–323
16. Mesland, D. A. (1992) Possible actions of gravity on the cellular machinery. *Adv. Space Res.* **12**, 15–25
17. Vorselen, D., Roos, W. H., MacKintosh, F. C., Wuite, G. J. L., and van Loon, J. J. W. A. (2014) The role of the cytoskeleton in sensing changes in gravity by nonspecialized cells. *FASEB J.* **28**, 536–547
18. Hänggi, P. (2002) Stochastic resonance in biology. How noise can enhance detection of weak signals and help improve biological information processing. *ChemPhysChem* **3**, 285–290
19. Singh, K. P., Kumari, R., and Dumond, J. W. (2010) Simulated microgravity-induced epigenetic changes in human lymphocytes. *J. Cell. Biochem.* **111**, 123–129
20. Wegener, J., Janshoff, A., and Galla, H. J. (1999) Cell adhesion monitoring using a quartz crystal microbalance: comparative analysis of different mammalian cell lines. *Eur. Biophys. J.* **28**, 26–37
21. George, T. F., Jelski, D., Letfullin, R. L., and Zhang, G. P. (2011) *Computational Studies of New Materials II*, World Scientific, Singapore
22. Roberts, W. E., Mozsary, P. G., and Klingler, E. (1982) Nuclear size as a cell-kinetic marker for osteoblast differentiation. *Am. J. Anat.* **165**, 373–384
23. Sugawara, Y., Kamioka, H., Honjo, T., Tezuka, K., and Takano-Yamamoto, T. (2005) Three-dimensional reconstruction of chick calvarial osteocytes and their cell processes using confocal microscopy. *Bone* **36**, 877–883
24. Chambliss, A. B., Khatau, S. B., Erdenberger, N., Robinson, D. K., Hodzic, D., Longmore, G. D., and Wirtz, D. (2013) The LINC-anchored actin cap connects the extracellular milieu to the nucleus for ultrafast mechanotransduction. *Sci. Rep.* **3**, 1087
25. Tamiello, C., Bouten, C. V. C., and Baaijens, F. P. T. (2015) Competition between cap and basal actin fiber orientation in cells subjected to contact guidance and cyclic strain. *Sci. Rep.* **5**, 8752
26. Cassidy, J. W., Roberts, J. N., Smith, C. A., Robertson, M., White, K., Biggs, M. J., Oreffo, R. O. C., and Dalby, M. J. (2014) Osteogenic lineage restriction by osteoprogenitors cultured on nanometric grooved surfaces: the role of focal adhesion maturation. *Acta Biomater.* **10**, 651–660
27. Biggs, M. J. P., Richards, R. G., Gadegaard, N., Wilkinson, C. D. W., and Dalby, M. J. (2007) Regulation of implant surface cell adhesion: characterization and quantification of S-phase primary osteoblast adhesions on biomimetic nanoscale substrates. *J. Orthop. Res.* **25**, 273–282
28. Maraldi, M., Valero, C., and Garikipati, K. (2014) A computational study of stress fiber-focal adhesion dynamics governing cell contractility. *Biophys. J.* **106**, 1890–1901
29. Schwarz, U. S., Balaban, N. Q., Riveline, D., Bershadsky, A., Geiger, B., and Safran, S. A. (2002) Calculation of forces at focal adhesions from elastic substrate data: the effect of localized force and the need for regularization. *Biophys. J.* **83**, 1380–1394
30. Ezratty, E. J., Partridge, M. A., and Gundersen, G. G. (2005) Microtubule-induced focal adhesion disassembly is mediated by dynamin and focal adhesion kinase. *Nat. Cell Biol.* **7**, 581–590
31. Wehrle-Haller, B., and Imhof, B. A. (2003) Actin, microtubules and focal adhesion dynamics during cell migration. *Int. J. Biochem. Cell Biol.* **35**, 39–50
32. Worofka, R., and Sauermann, G. (1978) Nuclear columns, kinetics of RNA synthesis and release in isolated rat liver nuclei. *Biochim. Biophys. Acta* **518**, 61–80
33. Wyrobek, A. J., Meistrich, M. L., Furrer, R., and Bruce, W. R. (1976) Physical characteristics of mouse sperm nuclei. *Biophys. J.* **16**, 811–825
34. Li, Y., Lovett, D., Zhang, Q., Neelam, S., Kuchibhotla, R. A., Zhu, R., Gundersen, G. G., Lele, T. P., and Dickinson, R. B. (2015) Moving cell boundaries drive nuclear shaping during cell spreading. *Biophys. J.* **109**, 670–686
35. Dahl, K. N., Ribeiro, A. J. S., and Lammerding, J. (2008) Nuclear shape, mechanics, and mechanotransduction. *Circ. Res.* **102**, 1307–1318
36. Brangwynne, C. P., Mitchison, T. J., and Hyman, A. A. (2011) Active liquid-like behavior of nucleoli determines their size and shape in *Xenopus laevis* oocytes. *Proc. Natl. Acad. Sci. USA* **108**, 4334–4339
37. Van Loon, J. J. W. A., van Laar, M. C., Korterik, J. P., Segerink, F. B., Wubbels, R. J., de Jong, H. A. A., and van Hulst, N. F. (2009) An atomic force microscope operating at hypergravity for in situ measurement of cellular mechano-response. *J. Microsc.* **233**, 234–243
38. Christophorou, N., Rubin, T., Bonnet, I., Piolot, T., Arnaud, M., and Huynh, J. R. (2015) Microtubule-driven nuclear rotations promote meiotic chromosome dynamics. *Nat. Cell Biol.* **17**, 1388–1400
39. Schaedel, L., John, K., Gaillard, J., Nachury, M. V., Blanchoin, L., and Théry, M. (2015) Microtubules self-repair in response to mechanical stress. *Nat. Mater.* **14**, 1156–1163
40. Neelam, S., Chancellor, T. J., Li, Y., Nickerson, J. A., Roux, K. J., Dickinson, R. B., and Lele, T. P. (2015) Direct force probe reveals the mechanics of nuclear homeostasis in the mammalian cell. *Proc. Natl. Acad. Sci. USA* **112**, 5720–5725
41. Pellegrin, S., and Mellor, H. (2007) Actin stress fibres. *J. Cell Sci.* **120**, 3491–3499
42. Liu, J., Wang, Y., Goh, W. I., Goh, H., Baird, M. A., Ruehland, S., Teo, S., Bate, N., Critchley, D. R., Davidson, M. W., and Kanchanawong, P. (2015) Talin determines the nanoscale architecture of focal adhesions. *Proc. Natl. Acad. Sci. USA* **112**, E4864–E4873
43. Swift, J., Ivanovska, I. L., Buxboim, A., Harada, T., Dingal, P. C. D. P., Pinter, J., Pajerowski, J. D., Spinler, K. R., Shin, J. W., Tewari, M., Rehfeldt, F., Speicher, D. W., and Discher, D. E. (2013) Nuclear lamin-A scales with tissue stiffness and enhances matrix-directed differentiation. *Science* **341**, 1240104
44. Ihalainen, T. O., Aires, L., Herzog, F. A., Schwartlander, R., Moeller, J., and Vogel, V. (2015) Differential basal-to-apical accessibility of lamin A/C epitopes in the nuclear lamina regulated by changes in cytoskeletal tension. *Nat. Mater.* **14** , 1252–1261
45. Qi, R., Xu, N., Wang, G., Ren, H., Li, S., Lei, J., Lin, Q., Wang, L., Gu, X., Zhang, H., Jiang, Q., and Zhang, C. (2015) The lamin-A/C-LAP2α-BAF1 protein complex regulates mitotic spindle assembly and positioning. *J. Cell Sci.* **128**, 2830–2841

Received for publication August 6, 2016.
Accepted for publication October 31, 2016.

THE FASEB JOURNAL
The Journal of the Federation of American Societies for Experimental Biology

Mechanical remodeling of normally-sized mammalian cells under a gravity vector

Chen Zhang, Lüwen Zhou, Fan Zhang, et al.

FASEB J published online November 8, 2016
Access the most recent version at doi:10.1096/fj.201600897RR

SUPPLEMENTAL FIGURES AND CAPTIONS

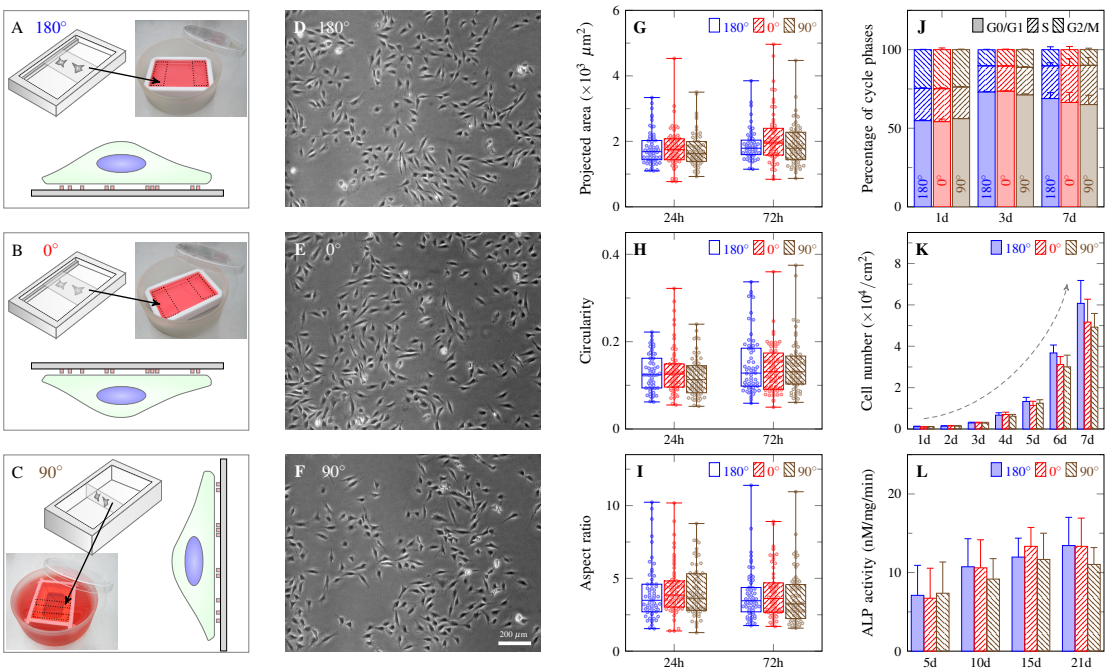

Figure S1. Mechanical stability and biological homeostasis of MC3T3-E1 cells grown in different oriented substrates. (A-C) Demonstration of upward- (A), downward- (B), or edge-on-oriented (C) substrate placed into a customer-made chamber (Arrows indicate the coverslips for cell growth). (D-F) Photo of cells grown at 180º (D), 0º (E), or 90º (F). Cell projected area (G), circularity (H), or aspect ratio (I), as well as cell cycle phase percentage (J), proliferation (K), and differentiation (L) are plotted on three orientations at given time points. Data are presented as the median value with 25th and 75th percentiles of 60 cells from three experiments (G-I) or as the mean value SE from two (J) or three (K-L) repeats.

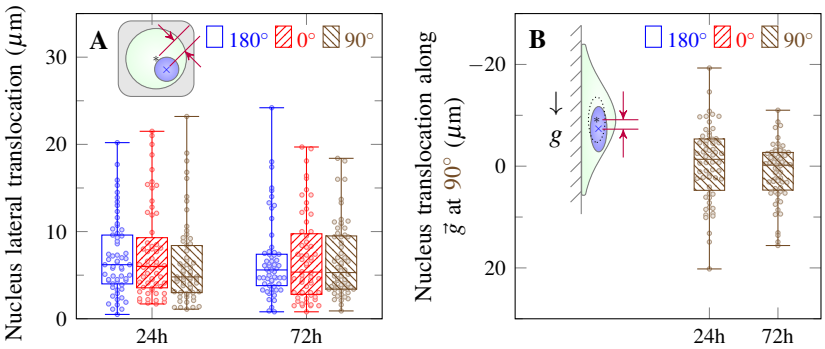

Figure S2. Distinct nucleus translocation in three orientations. Lateral translocation of nucleus is defined as the lateral distance between nucleus centroid (×) and cell centroid (*) on projected x-y plane (insert in A). Translocation on E is specifically defined as the distance between nucleus and cell centroids along gravity vector (insert in B). Data are presented as the median value with 25th and 75th percentiles of 60 cells from three experiments.

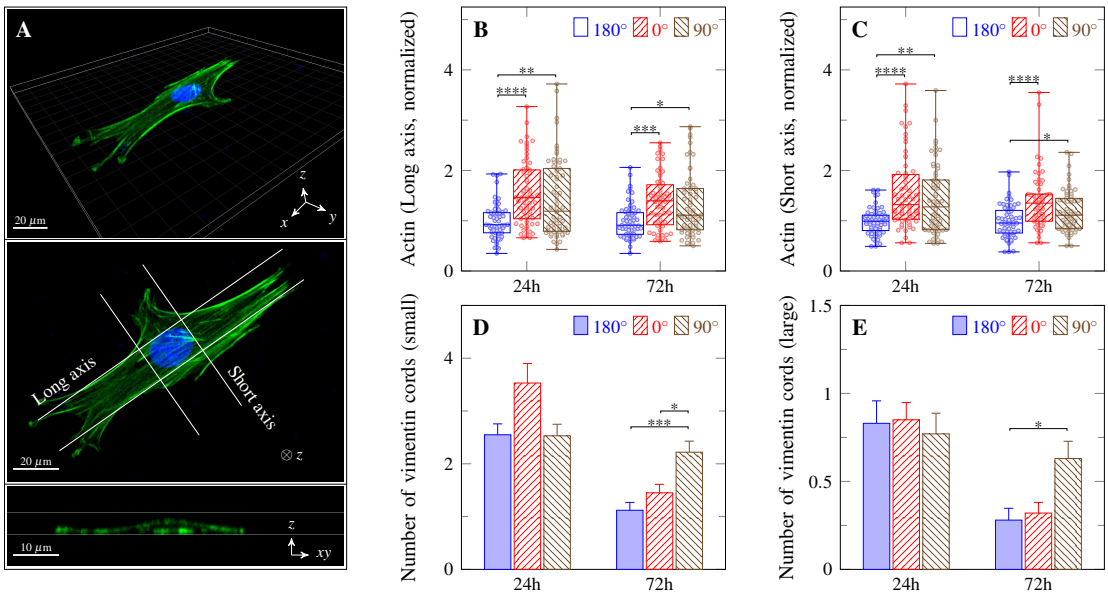

Figure S3. 3D perinuclear cytoskeletal analysis. A typical 3D reconstructed image (upper) is illustrated from top (middle) or side view (lower) of nucleus periphery (A). Perinuclear actin expression along the long- (B) or short-axis (C) is normalized to the ones at 180º and vimentin cord number is counted on small (D; <2.5 μm^2) or large (E; ≥2.5 μm^2) size. Data are presented as the median value with 25th and 75th percentiles of 60 cells from three experiments. *, **, ***, ****: p< 0.05, 0.01, 0.001, 0.0001.

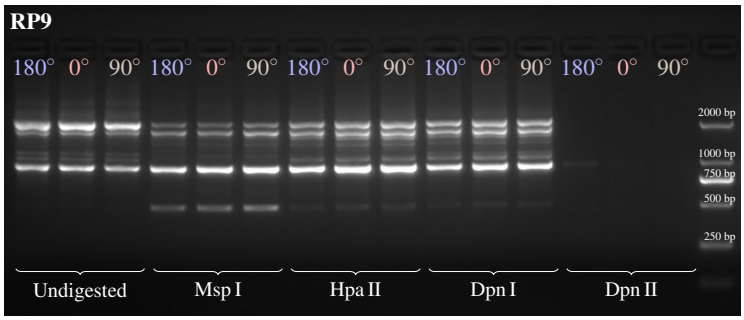

A list of Primers Used for RAPD Analyses.

Primer	Sequence(5'-3')
RP1	GGGGGTCTTT
RP2	GAACGGACTC
RP3	GTCCCGACGA
RP4	AAAGCTGCGG
RP5	GACGGATCAG
RP6	CACACTCCAG
RP7	TTCCCCCCAG
RP8	GTTGCCAGCC
RP9	ACTTCGCCAC

Figure S4. Representative RAPD fingerprints in three orientations. Genomic DNA isolated from cells placed and grown up at 180º, 0º, or 90º at 24 h (those data at 72 h are not shown) was digested with methylation insensitive (Msp I) or sensitive restriction enzymes (Hpa II, Dpn I and Dpn II), and used for RAPD amplifications as described in Materials and Methods. None of the 9 random primers (right table) used reveals any significant change in DNA fingerprints.

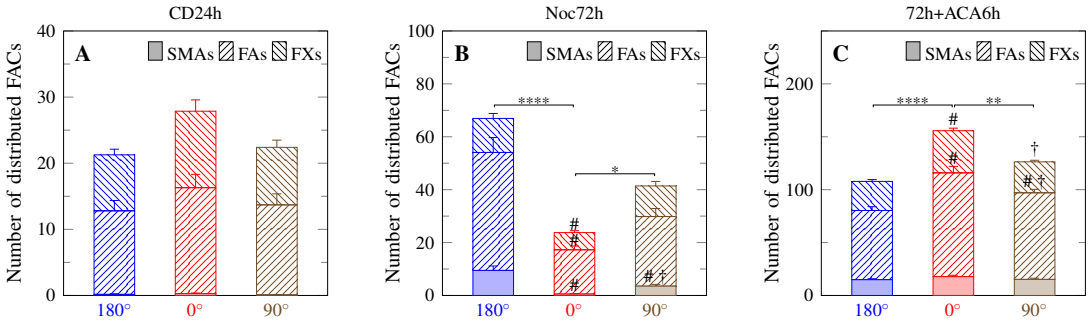

Figure S5. Mechanical remodeling of cytoskeleton-treated cells in three orientations. Distribution of differentially sized FACs are plotted against three orientations for cells treated by cytochalasin D for 24 h (A), by nocodazole for 72 h (B) or by acrylamide for additional 6 h (C). Data are presented as the mean value ± SE of 30-45 cells from three experiments. *, **, ****: $p < 0.05$, 0.01, 0.0001; $^{\#}$ and †: $p < 0.05$ as compared to those at 180º and 0º, respectively.

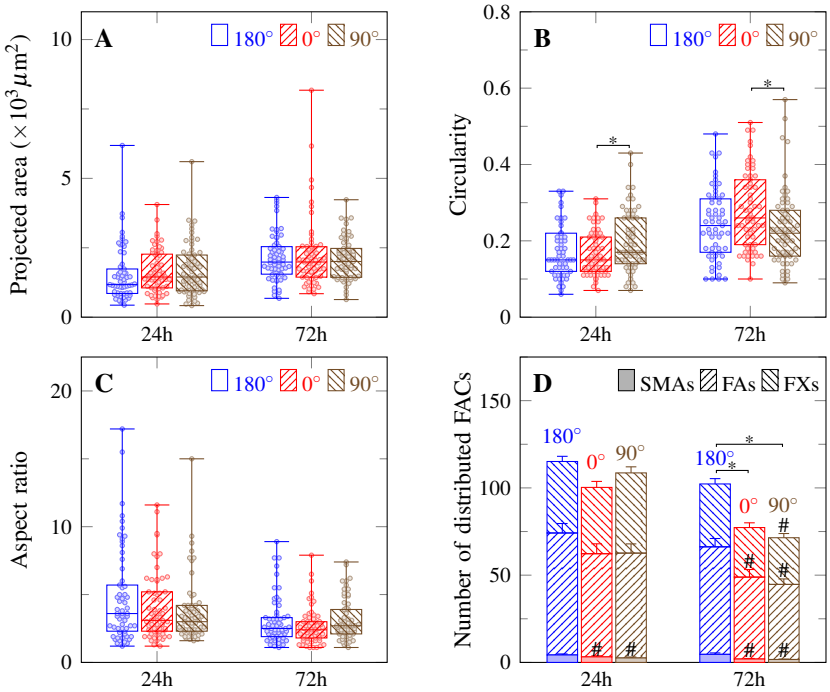

Figure S6. Morphological and mechanical remodeling of Y-27632-treated cells in three orientations. Cell projected area (A), circularity (B), or aspect ratio (C), as well as number distribution of differentially sized FACs (D) are plotted against three orientations. Data are presented as the median value with 25th and 75th percentiles (A-C) or as the mean value ± SE (D) of 60 cells from three experiments. *: $p < 0.05$; $^{\#}$: $p < 0.05$ as compared to that at 180º.